

Fiber Optic Sensors-Based Thermal Analysis of Perfusion-Mediated Tissue Cooling in Liver Undergoing Laser Ablation

Elena De Vita , Martina De Landro , Carlo Massaroni , Agostino Iadicicco , Paola Saccomandi , Emiliano Schena , and Stefania Campopiano 

Abstract—The current challenge in the field of thermo-ablative treatments of tumors is to achieve a balance between complete destruction of malignant cells and safeguarding of the surrounding healthy tissue. Blood perfusion plays a key role for thermal ablation success, especially in the case of highly vascularized organs like liver. This work aims at monitoring the temperature within perfused swine liver undergoing laser ablation (LA). Temperature was measured through seven arrays of Fiber Bragg Grating sensors (FBGs) around the laser applicator. To mimic reality, blood perfusion within the *ex-vivo* liver was simulated using artificial vessels. The influence of blood perfusion on LA was carried out by comparing the temperature profiles in two different spatial configurations of vessels and fibers. The proposed setup permitted to accurately measure the heat propagation in real-time with a temperature resolution of 0.1 °C and to observe a relevant tissue cooling near to the vessel up to 65%.

Index Terms—Blood perfusion, fiber Bragg gratings, laser ablation, temperature monitoring, thermal ablation.

I. INTRODUCTION

THE goal of any cancer therapy is a complete destruction of malignant cells, including a safety margin ranging from 5 to 10 mm. Actual ablative systems are able to coagulate tumor tissue precisely up to a diameter of 3.0 - 3.5 cm [1], [2]. However, sparing healthy tissues that surround the tumor from thermal damage plays a pivotal role in the achievement of a controlled thermo-ablated volume [3]. Among the available cancer treatments, thermo-ablative technology offers several advantages

over surgical resection: most notably, lower morbidity, increased preservation of surrounding tissues, reduced costs and shorter hospitalization times, as well as the ability to treat patients who are not candidates for conventional therapies [4], [5]. The success of high-temperature hyperthermia depends on the thermal dose delivered to the cancerous tissue during the treatment, which is related to both exposure time and temperature, since as the tissue temperature increases, the amount of time needed to achieve the desired thermal lesion exponentially decreases [6]–[9]. Anyway, there are other physical, physiological and biochemical factors which must be also considered in evaluating the effectiveness of thermal ablation in cancer therapy [10]. Temperature distribution generated in the ablated area during thermal coagulation for cancer therapy depends on the energy balance between the power density produced (related to the energy deposition by the source and the metabolism) and the dissipated one via energy losses, mainly due to blood perfusion and water evaporation terms [11], [12]. Therefore, the deposition of energy in cancerous tissues during thermal ablation is influenced by factors like thermoregulation and metabolism, differential thermal sensitivity, properties of the source and blood perfusion. In particular, it has been observed that the major energy loss mechanism in thermo-ablative treatments is represented by the blood flow, especially in large vessels [13], [14].

Thermal ablation comprises several distinct techniques, which can be classified according to the type of energy source applied, including laser, radiofrequency current, microwave and ultrasound [15]. This work is focused on Laser Ablation (LA), which relies on the coagulation of the tissue induced by the insertion of a light-conducting quartz fiber into the tumor region. During LA, the laser light locally heats the target tissue causing coagulative necrosis, secondary degeneration and atrophy in the tumorous cells [16]. For this thermo-ablative technique, the size of the heated volume has been observed to be affected by the blood perfusion. The latter causes the so-called heat sink effect, consisting in a rapid dissipation of heat and a significant cooling of the tissue due to phenomena described by the heat convection coefficient of blood vessels [17]. Therefore, to have uniform heating of the tumor, the consideration of vascularity assumes major importance, especially when the treated organ is the liver. Indeed, the blood perfusion due to the high hepatic vascularization, the pathological angiogenesis of cancer and

Manuscript received April 21, 2020; revised June 9, 2020; accepted June 14, 2020. Date of publication June 25, 2020; date of current version February 19, 2021. This work was supported in part by the European Research Council (ERC) under the European Union's Horizon 2020 Research and Innovation Program (GA n. 759159), in part by Fondazione Cariplo, Grant 2017-2075, and in part by the University of Naples "Parthenope" through the "Bando di sostegno alla ricerca individuale per triennio 2015-2017, Annualità 2017". (Corresponding author: Elena De Vita.)

Elena De Vita is with the Department of Engineering, University of Naples "Parthenope", Naples 80143, Italy (e-mail: elena.devita@uniparthenope.it).

Martina De Landro and Paola Saccomandi are with the Department of Mechanical Engineering, Politecnico di Milano.

Carlo Massaroni and Emiliano Schena are with the Università Campus Bio-Medico di Roma.

Agostino Iadicicco and Stefania Campopiano are with the Department of Engineering, University of Naples "Parthenope".

Digital Object Identifier 10.1109/TBME.2020.3004983

the subsequent heat sink effect prevent the temperature rising to cytotoxic levels [18], so that tumor recurrence occurs more frequently when the hepatic tumor is localized next to a vessel [19]. For this reason, the knowledge of the effects due to the presence of a blood vessel on the extent of thermal damage represents a relevant information for better understanding the LA efficacy.

Along this line, given the clinical relevance of the blood perfusion influence on the success of LA therapy, this work aims to experimentally analyze and evaluate the temperature map reached by the ablated tissue in presence of a blood vessel. In thermal ablation scenario, several thermometric methods have been explored to provide a temperature feedback during thermal ablation therapies. Unfortunately, 3D non-invasive thermometry for control of thermo-ablative systems is beyond the present capability of imaging systems, hence thermal dosimetry using invasive thermometry is an absolute necessity to determine the temperature distributions achieved [20]. Among the different techniques, Fiber Bragg Grating sensors (FBGs) stand out from invasive thermometry techniques, such as thermocouples, thermistors and fluoroptic sensors, for their characteristics of biocompatibility, immunity to electromagnetic interference, non-toxicity and chemical inertness, that guarantee no immunity response from human defense system and a type of sensor intrinsically safe for the patient [21]–[23]. Another advantageous characteristic of FBGs consists in their capability of multiplexing, that means several gratings can be integrated within a single optical fiber creating an array of sensors. This property allows recording multi-point measurements by inserting only one fiber, i.e. an array of FBGs, within the organ, ensuring a minimally invasive thermometric solution with high spatial resolution.

This article presents an experimental study of the temperature field inside the target lesion during LA in a perfused swine *ex-vivo* liver. An FBG-based system is proposed for measuring tissue temperature in thirty-five points in the volume around the laser fiber, obtaining a considerable number of measurement sites in the target lesion. In line with the state-of-the-art [23]–[28], this work demonstrates that the proposed setup allowed to effectively study, monitor and accurately measure the heat propagation inside the liver tissue undergoing LA in real-time, with a temperature resolution of 0.1 °C. However, the groundbreaking aim of this study was to demonstrate that the proposed experimental setup allowed to observe, investigate and quantify the variation of the temperature field in the target region of the LA treatment when the laser applicator is inserted nearby a blood vessel. The obtained temperature mapping lays the foundation for further *in-vivo* investigations in these field, which could be beneficial for several reasons: i) to support the surgeon during the treatment; ii) to adjust the treatment settings in order to control the thermal damage also during blood perfusion; and iii) to provide an adequate thermal lesion to the target while sparing the surrounding healthy tissue.

II. EXPERIMENTAL SETUP

In this section the experimental setup used to investigate the damaged zone in *ex-vivo* swine livers (4 hours fresh) undergoing

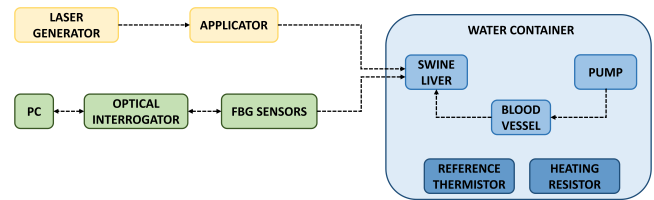


Fig. 1. Schematic of the experimental setup. The laser instrumentation is represented in yellow, the optical equipment for temperature measurements in green and the organ perfusion system in blue.

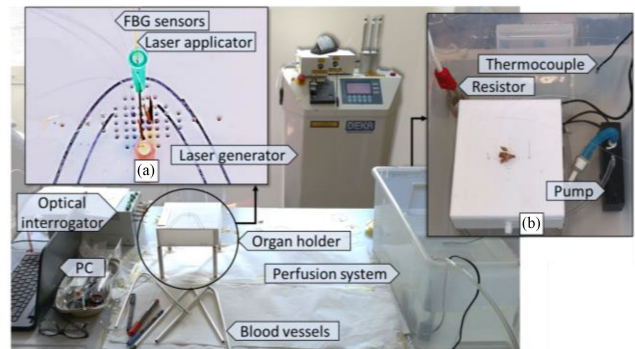


Fig. 2. Picture of the experimental setup before doing the experiment, so the organ holder was still empty, and the blood vessels were not yet inserted in the organ. a) Detail of laser fiber applicator and fiber optic sensors inside the organ holder. b) Detail of the perfusion system during the tests: vessels were inserted in the organ, which was into the holder.

simulated blood perfusion during LA is described, schematically reported in Fig. 1, and illustrated in Fig. 2.

A. Laser Instrumentation

LA was performed using a Nd:YAG laser system with a wavelength of 1064 nm, operating in a CW regime (Smart 1064 BS, Deka M.E.L.A. Srl, Florence, Italy). A power of 2 W was delivered to the organ through the laser applicator, consisting of a quartz optical fiber (bare fiber, numerical aperture 0.22, Asclepion Laser Technologies) with 300 μm core diameter, inserted in the tissue at a depth of 1 cm. A cannula is used to assist the insertion of the laser fiber and after the proper positioning of laser tip the cannula is extracted. The duration of the laser discharge was 5 min, in such a way as to release 600 J of energy for each trial. This energy setting is typical of clinical applications of laser ablation for tumor treatment [29].

B. Optical Equipment for Temperature Measurements

The temperature distribution during each LA treatment was monitored using 7 arrays of bare FBGs, denoted by the letters from A to G, properly positioned in the volume surrounding the tip of the laser applicator. FBGs act as band rejection filters, which reflect a narrow range of wavelengths centered around the so-called Bragg wavelength [30]–[32] given by:

$$\lambda_B = 2 \cdot n_{eff} \cdot \Lambda \quad (1)$$

where n_{eff} is the effective refractive index (RI) of the fundamental mode propagating in the fiber core, and Λ is the spatial

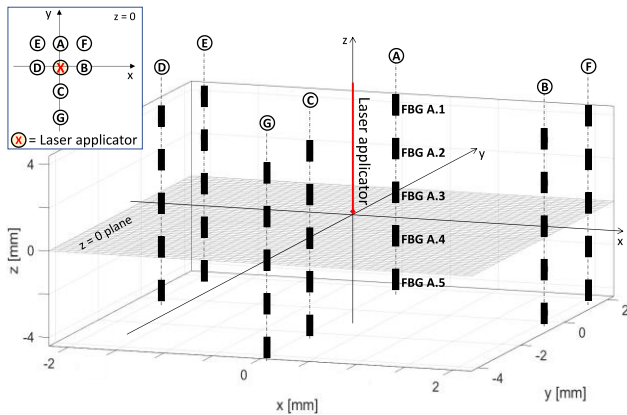


Fig. 3. Schematic of FBG arrays positioning around the laser applicator in the reference coordinate system in the case of laser tip positioning at the same depth of the third FBG sensor of each array along the z-axis (not to scale). Top left figure represents the top-view arrangement of the arrays in the x-y plane. Laser fiber tip represents the origin of the coordinate system.

period of the grating. Bragg wavelength shifts if the effective RI or the grating periodicity is changed because of some perturbation, typically strain and temperature. Therefore, these external physical parameters are detected through the measurement of the shifted reflected wavelength. Since in this application the parameter of interest is represented by the temperature, FBGs were employed in a strain-free configuration; consequently, the relationship between Bragg wavelength shift and temperature changes ΔT is [30], [31]:

$$\Delta\lambda_B/\lambda_B = S_T \cdot \Delta T \quad (2)$$

where S_T is the thermal sensitivity of the grating.

For the wavelength shift detection, an optical spectrum analyzer (Model FS-22 HBM BraggMETER) was used. This data acquisition system is characterized by a tunable laser source and detector in the range 1500 ÷ 1600 nm and is equipped with eight optical channels. The optical interrogator measures λ_B with a minimum frequency of 1 Hz and with a resolution of 1 pm, allowing for measurements of temperature with a resolution of 0.1 °C.

Each array of sensors was composed by 5 FBGs (1 mm long with an edge-to-edge distance of 1 mm) for a total number of 35 sensing points, and the thermal sensitivity S_T of the sensors was $6.5 \cdot 10^{-6} \text{ }^\circ\text{C}^{-1}$. The FBG array positioning in the thermo-ablated volume is shown in Fig. 3, which shows a setup configuration in which the laser tip was positioned at the same depth of the third FBG of each array along the z-axis. The origin of the coordinate system is fixed in correspondence of the laser applicator tip. Each grating was denoted by the letter of the corresponding array and a progressive number starting from the top of the z-axis. For the sake of clarity, the axes are not reported to scale. The transversal distance among one array and the next one is 2 mm, except for array A and C, among which the laser fiber is placed, resulting in a high spatial resolution setup. In fact, since in LA the thermal gradient is particularly significant close to the applicator, a temperature measurement with high spatial resolution is mandatory to reconstruct the temperature

TABLE I
SPATIAL COORDINATES OF THE FBG ARRAYS IN $z = 0$ PLANE

FBG array	Coordinates in $z = 0$ plane	
	x [mm]	y [mm]
A	0	2
B	2	0
C	0	-2
D	-2	0
E	-2	2
F	2	2
G	0	-4

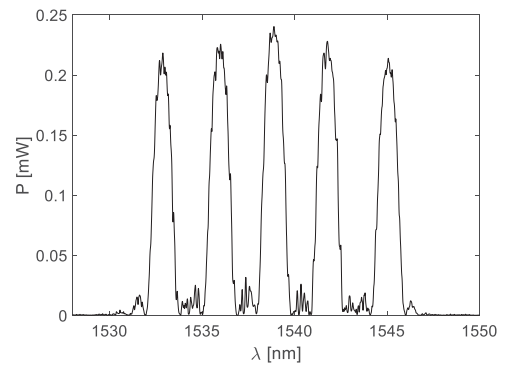


Fig. 4. Optical reflected spectrum of the array A.

map within the tissue. Table I lists the coordinates of the arrays in $z = 0$ plane. These spatial points are graphically represented in the top-left detail of Fig. 3 to specify how the arrays of sensors are positioned in the plane containing the laser applicator tip ($z = 0$ plane). As an example, the optical reflected spectrum of array A is shown in Fig. 4.

C. Organ Holder

The critical issue in these experiments is the difficulty to control the relative positions between fiber sensors and laser applicator inside the tissue. To overcome this hurdle, a custom holder was designed and fabricated, as shown more in detail in Fig. 5.

It consists in a PTFE box with size of 16x16x6 cm (LxWxH) to host the organ. The upper and the lower sides of the holder were characterized by dense holes matrix (hole diameter of 1.0 mm and holes center distance of 2.0 mm) allowing to set the vertical position of the optical fibers (of sensors and laser) going through the organ.

The fibers of sensors and laser applicator were inserted into the organ through needles and a cannula, respectively. The depth of each fiber in the liver tissue was controlled by means of a reference mark on them. After the positioning of sensors and applicator, the needles were extracted from the lower side of the organ holder, leaving the sensors in the tissue, whereas the cannula, used to insert the laser applicator, was retracted upward to leave the laser tip in contact with the liver tissue.

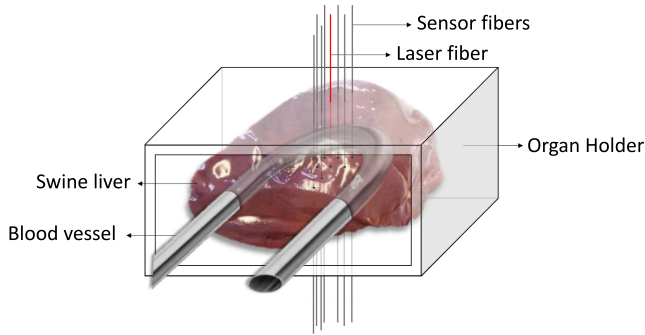


Fig. 5. Schematic of the organ holder containing the swine liver undergoing LA, with vessel and fibers of sensors and laser applicator placed inside.

D. Perfusion System

To simulate the blood perfusion in the liver, a system made of pump, heating resistance and blood vessels was used (Fig. 2). The influence of the perfusion on the tissue temperature undergoing LA was evaluated by simulating two types of blood vessels using two aluminum tubes with the same thickness (i.e., 1 mm) and different inner diameters (i.e., 4 mm and 6 mm), according to the main values retrieved for adult human liver vasculature in normal conditions. Indeed, the chosen diameters mimic the left and right branches of the portal vein [33]–[35]. These tubes were arranged in “U”-shape, to partially surround the ablation and the measurement zone (Fig. 5). The length of the tubes used as blood vessels is 50 cm, but only a fraction of such length was inserted in the *ex-vivo* livers, the one corresponding to the U-bent, as schematically reported in Fig. 5. To better mimic reality, the liver was immersed in water at 37 °C. As a temperature reference, a thermocouple was kept in the water during the performed tests. The pump allowed the water flow through the blood vessel, inserted in the liver thanks to a pointed tip, with a flow rate of 0.64 l·min⁻¹ and 0.44 l·min⁻¹ for the 4 mm and 6 mm diameter tube, respectively. These flowrates aim at achieving a uniform temperature in the aluminum tube.

III. RESULTS

This section reports and discusses the experimental results, i.e., the temperature profiles measured in the thirty-five measurement sites and the effects of the simulated blood perfusion on the target undergoing LA.

A. Temperature Maps

Fig. 6 shows the array A temperature map along the *z*-direction (vertical axis in the graph) versus time (horizontal axis) during a representative laser discharge in which array A recorded the maximum temperature values. The blood perfusion was simulated through the aluminum tube (vessel) with 4 mm inner diameter. A piecewise linear interpolation was applied on the temperature experimental points to estimate the temperature profile. The laser discharge lasted five minutes. The recorded temperature values are in accordance with the relative position of sensors and laser fiber tip: the highest temperature was measured

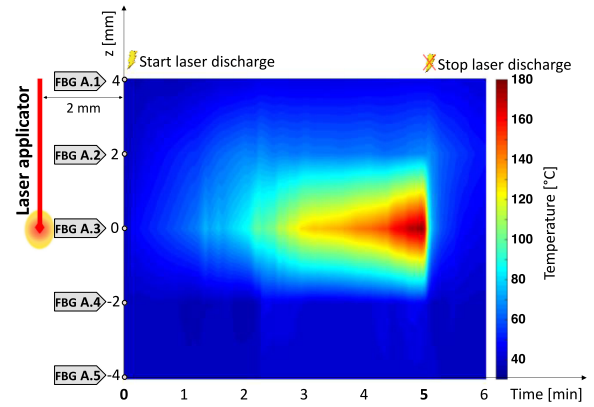


Fig. 6. Temperature profile of the five FBGs along array A during LA.

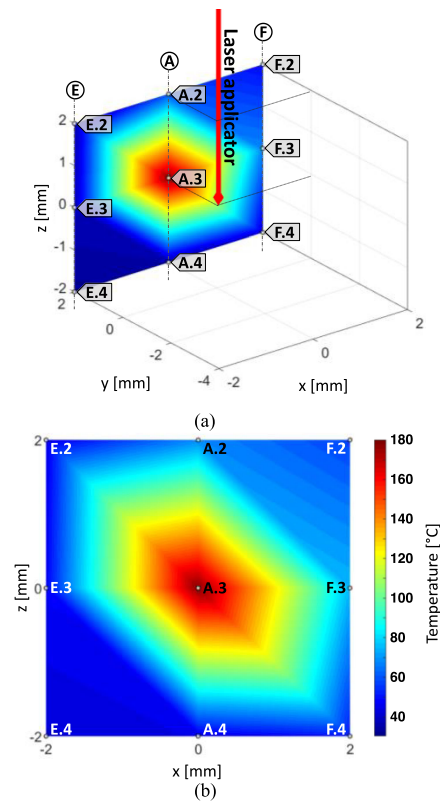


Fig. 7. (a) Spatial arrangement of arrays A, E and F with respect to the laser fiber. (b) Temperature map in $y = 2$ mm plane obtained from the experimental temperature values measured by the second, the third and the fourth FBG of arrays A, E and F; experimental data points are indicated by grey dots.

by the sensor closest to the laser fiber tip (FBG A.3). This also applies to the other FBG arrays: for each array, the central sensor recorded the maximum temperature.

Finally, it can be observed that as the laser was turned-off, from the fifth minute, temperature fastly decays.

The multidimensional temperature monitoring system allowed to estimate and visualize 2D temperature maps during the ablation treatment. For the purpose, in Fig. 7(a) and 7(b) the temperature map obtained at the end of the laser discharge in $y = 2$ mm plane during the same test of Fig. 6 is showed. In

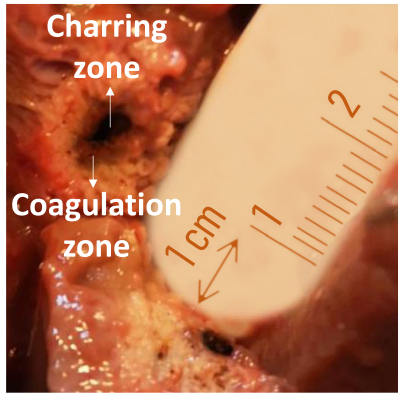


Fig. 8. Laser ablation effect on *ex-vivo* swine liver. Normal tissue is red pink; in contrast, the ablated region is characterized by three concentric zones: the central one is black and denotes the carbonization of the tissue in correspondence of the laser fiber tip, then a zone lighter than the charring one but darker than the healthy tissue, due to the coagulation phenomenon, can be seen, and finally the external tissue annulus is pale white because of the protein denaturation.

particular, in Fig. 7(a) the spatial arrangement of arrays A, E and F with respect to the laser fiber is reported; Fig. 7(b) shows the temperature map in $y = 2$ mm, containing the second, the third and the fourth FBG of the arrays. Temperature is reported by a colormap versus spatial axes and it was achieved with a linear interpolation of the experimental data points. The highest temperature was reached by FBG A.3, which recorded 177.3 °C.

In Fig. 8, a picture of the ablated dissected sample of the swine liver at the end of one of the treatments is reported in order to macroscopically evaluate the thermal ablation process. It shows the charring and the coagulation phenomena, in the region surrounding the laser tip and in the area all around it, respectively.

B. Effects of the Blood Perfusion

This section is focused on the perfusion effects on the tissue heating treated by LA procedure. In particular, two cases with different vessel tube size and sensors arrangement are investigated.

Fig. 9(a) shows a schematic of the top-view (x - y plane) of the first experiment. The vessel was symmetrically positioned with respect to the fibers for laser and sensors. The distances $d_x = 0.7$ cm and $d_y = 0.3$ cm were measured at the end of this experiment, by cutting the tissue sample. For this experiment, the tip of the laser fiber, which corresponds to the origin of the coordinate system, as well as the vessel are arranged at same depth (z position) of the second FBG of each array.

Fig. 9(b) plots the temperature profiles of array E and F versus time: the curve color identifies the z -position of gratings, whereas array E and F are plotted with continuous and dotted lines, respectively. Moreover, Fig. 9(c) shows the temperature maps during the same experiment for both arrays.

The maximum temperatures were achieved by E.2 and F.2, as can be seen in Fig. 9(b) and 9(c). As evident, due to the symmetry of the vessel and sensors configuration, the temperature profiles of the gratings at the same depth (same z -position) are very

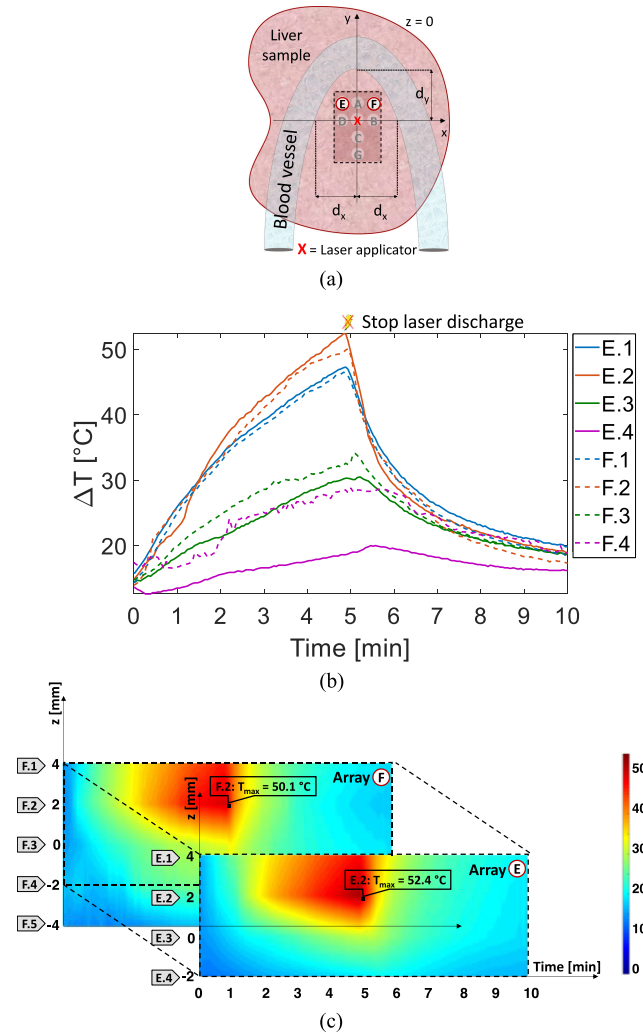


Fig. 9. Symmetric configuration of blood vessel, laser applicator and sensor fibers. (a) Schematic of blood vessel and FBG position in $z = 0$ plane during one of the performed tests, in which the laser tip was positioned at the same depth of the second FBG of each array along the z -axis. The distances between the blood vessel and the arrays are not in scale. (b) Temperature variation of array E and F sensors during the treatment. (c) Temperature maps along the z -direction (vertical axis) versus time (horizontal axis) registered by the sensors of array E and F.

similar, especially when the registered temperatures are elevated (Fig. 9(b)). Indeed, for example, the maximum temperature variations of E.2 and F.2 are 52.4 °C and 50.1 °C, respectively. Moreover, considering E.1 and F.1, the difference between the maximum temperature variations is even lower (<1 °C).

In Fig. 10, a different laser discharge is analyzed. In this case the laser tip was located at the same depth of the fourth FBG of each array along the z -axis. The main difference from the previous discharge described in Fig. 9 consists in the asymmetry of the blood vessel positioning with respect to the position of the arrays: as reported in the schematic of Fig. 10(a), the aluminum tube was not centered with respect to the ablation and the measurement area: $d_{x,1} = 0.5$ cm, $d_{x,2} = 3.0$ cm and $d_y = 1.1$ cm were measured. Therefore, array E is the closest one to the vessel.

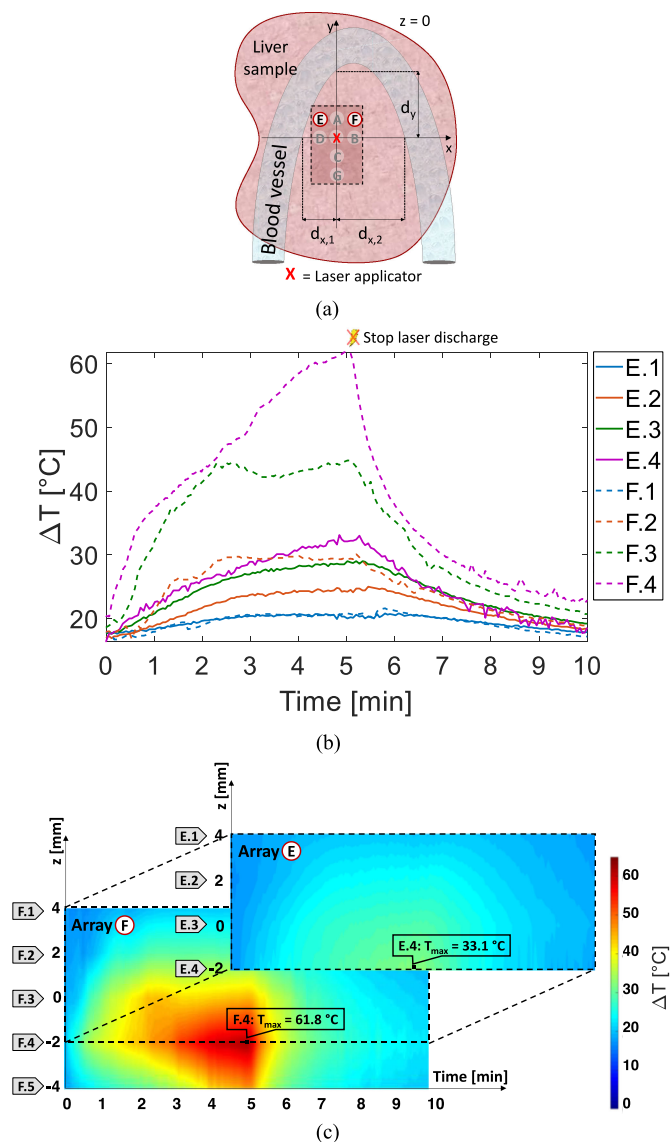


Fig. 10. Asymmetric configuration of blood vessel, laser applicator and sensor fibers. (a) Schematic of blood vessel and FBG position in $z = 0$ plane during one of the performed tests in which the laser tip was positioned at the same depth of the fourth FBG of each array along the z-axis. (b) Temperature variation of array E and F sensors during the treatment. (c) Temperature maps along the z-direction (vertical axis) versus time (horizontal axis) registered by the sensors of array E and F.

The asymmetry of the problem allowed to compare the temperature profiles of the sensors at the same distance from the laser tip, but at different distances from the blood vessel. This analysis allows quantifying the blood perfusion influence on the temperature map in the ablated area. Temperature profiles measured by all the sensors are plotted in Fig. 10(b), whereas the color maps are plotted in Fig. 10(c). As expected, due to the vessel proximity, array E gratings measured lower temperatures than the correspondent gratings of array F, particularly E.4 and E.3, whose maximum temperature variation was respectively 28.7 °C and 15.8 °C less than F.4 and F.3. A similar behavior was observed in the temperature profiles of array B and D. These arrays were both positioned next to the laser fiber, so in

general the temperature reached higher values, but even though they were symmetric with respect to the ablation source, they recorded completely different temperatures. Indeed, the highest temperature value reached by B.4 was 102.8 °C, whereas the maximum value of the corresponding grating D.4, closer to the vessel, was only 39.9 °C. The difference in the temperature values measured by array E and F is highlighted in Fig. 10(c), where the temperature maps of the two arrays during the laser discharge are displayed, contrary to what happens in the symmetric case showed in Fig. 9(c).

The evidence emerging from these experiments demonstrates that the used setup was able to measure a significant cooling effect in the ablated zone due to the blood perfusion when the vessel is located ~ 0.5 cm far from the laser applicator.

IV. DISCUSSION

The cooling phenomenon observed in Section III impairs a uniform heating of the tumor, especially in an organ like liver, in which the blood perfusion is not negligible. In fact, compared with other organs, the liver vasculature is unique due to the two blood sources: the hepatic artery, which supplies the liver with oxygenated blood, and the portal vein, which collects partially deoxygenated blood from the intestinal tract including spleen and pancreas [35]. Although it is generally assumed that the poorly organized vascular bed into the tumor probably cause only minimal tissue cooling and thus minimal lesion reduction, the tumor is surrounded by well perfused liver parenchyma and it is here that the cooling effect is mainly exerted [36]. In such a situation there is a good chance that there will be underdosed areas and that the tumor will grow from these areas around the vessels and from the peripheral tumor tissue within few weeks [20], [37].

Many strategies to alleviate this dissipating effect have focused on the reduction of hepatic blood flow with a systemically administered pharmacologic agent or a vascular occlusion of the hepatic inflow [17], [38]. Chen *et al.* investigated the variation of the lesion diameter during high-intensity focused ultrasound therapy with either normal blood flow or reduced blood flow by ligation of both the hepatic artery and portal vein [39]. They observed that the lesion diameter with normal blood flow was reduced by 20% compared with that made with both the hepatic artery and portal vein clamped. Heisterkamp *et al.* investigated increasing of the thermal necrosis area during interstitial laser coagulation by occluding the portal flow, observing intrahepatic lesions 4-5 cm in diameter in an *in-vivo* swine model [40]. A similar result was obtained by Muralidharan *et al.*, who modulated the hepatic blood flow during interstitial laser thermo-therapy achieving a greater destruction of tumor cells at the tumor-host interface [18]. In all these studies the evaluation of blood perfusion effects was only conducted by relying on a macroscopic qualitative detection of the whitish color change of the coagulated tissue, by which the extent of the lesion was determined.

There are studies in literature that investigate the importance of the blood vessel cooling effect during thermal ablation. Pillai *et al.* reported high local recurrence rates for tumors adjacent

to major hepatic vessels during treatments of radiofrequency and microwave ablation [41]. Tests were carried out on *ex-vivo* calf livers, comparing ablation efficacy in presence and absence of the vessel perfusion. Similar experimental studies were conducted also during multipolar radiofrequency ablation on *ex-vivo* perfused porcine livers by Poch *et al.*, who discovered a distinctive impact of the applicator-vessel distance on the shape of the ablation area [42]. However, there is only little information about the blood perfusion influence on the temperature distribution in the target region during LA, since ablation and coagulation properties are recognized and evaluated by the observation of the change in color from deep brownish red to grayish pink when native tissue was ablated [43]. In some cases, temperature was measured relying on thermocouples usually integrated in the radiofrequency and microwave probes [41].

Since the first *in-vivo* experiments proposed by Rao *et al.*, the use of FBGs for thermal treatments monitoring has gained widespread interest [44]. Currently, only few studies have investigated the feasibility for distributed FBG-based temperature monitoring in *in-vivo* LA tests on porcine livers [45], [46], but focusing on different aspects such as the measurement artifact due to patient's respiratory movements, without a quantitative blood perfusion analysis. A preliminary simulation of a real condition of blood perfusion was carried out on *ex-vivo* perfused animal organs, i.e. bovine kidney and porcine liver tissues, undergoing radiofrequency ablation [47].

As a novelty, the proposed FBG-based setup offered a dense sensing area, i.e. thirty-five measurement sites distributed around the laser applicator and partially located between applicator and vessel. To observe and quantify the thermal influence of the blood flow at constant temperature on LA efficacy, heated water at 37 °C was used to simulate both body temperature and blood flow, since blood predominantly consists of water and their thermal conductivity and specific heat are quite similar. Vessels were simulated through aluminum tubes, which stiffness allowed an easy insertion of the vessel in the tissue, after pointing the tip, and a controlled positioning with respect to laser applicator and sensors. The chosen diameters for aluminum tubes simulating the blood vessels are in accordance with the real dimensions of the left and right branches of the portal vein. Additional improvements in the perfusion system and in the materials used for the vessel simulation should be performed to better mimic the tissue of a real blood vessel. However, such an experimental setup brought to the elaboration of multidimensional temperature maps, which showed in real-time the temperature distribution in time and space (see Fig. 6 and Fig. 7, respectively) during ablation, and how it changed depending on the blood vessel distance from the laser applicator, as shown in Fig. 9(c) and Fig. 10(c). The analysis of an asymmetric spatial configuration of vessel and fibers and the comparison with respect to the symmetric one allowed to observe and quantify the inhomogeneity of the temperature distribution due to the vessel. A decrease in maximum temperature variation up to 65% can be noticed within 0.2 cm from laser tip.

Despite the distance from the clinical reality of the ablative treatments, *ex-vivo* trials could represent a chance to obtain controlled experiments and no artifacts due to patient's

respiratory movements, useful characteristics to conduct preliminary explorative tests [21], [41], [48]. In the applicative scenario discussed in this work, studying the influence that one large vessel can have on the temperature map in the healthy tissue could be the first step to isolate the blood perfusion role in a LA treatment and to investigate it. However, further tests in *in-vivo* case are needed to confirm and better investigate the cooling phenomenon of the ablation targeted area in presence of a real blood vessel. Moreover, further studies of perfusion effects on different techniques of thermal ablation, such as microwave and radiofrequency ablation, could be interesting in order to compare them with respect to LA in terms of treatment efficacy.

V. CONCLUSION

Local ablative therapies (like microwave, radiofrequency, and laser ablation) are gaining relevance in the treatment of hepatic malignancies. Only 40% of patients with hepatic malignancies are suitable for surgical resection at the time of diagnosis. Therefore, local ablative therapies play an important role in the treatment planning of these malignancies. So far, tumor ablation is limited by tumor size and vascular cooling effects. In fact, as the liver is highly vascularized because of a dual hematic supply represented by portal vein and hepatic artery and a thick network of blood vessels, blood perfusion represents an important parameter to consider in the assessment of thermal ablation treatments. In this work an experimental analysis of the blood perfusion effects on the temperature distribution in *ex-vivo* swine liver tissues undergoing LA has been performed. The blood perfusion of the liver was simulated by means of an ad-hoc system made of pump, heating resistance and blood vessels. To observe the influence of the perfusion settings on the temperature distribution in the tissue, two types of blood vessels have been simulated using two aluminum tubes with inner diameters of 4 mm and 6 mm, respectively.

The experimental results showed a relevant change in the temperature field between the laser tip and the blood vessel, whereas no significant difference between the two types of blood vessels was noticed. The temperature profiles obtained in two different spatial configurations of vessels and fibers of sensors and laser have been compared. When the vessel was symmetrically positioned with respect to the fibers, the temperature values measured by the arrays at the same distance from the laser tip were very similar (the difference between the maximum values was 2.3 °C). Differently, when the relative position of vessel and fibers was asymmetric, the FBG arrays closer to the vessel recorded a decrease of the maximum temperature variation from 28.7 °C to 62.9 °C (i.e. from 30% to 65%) with respect to the symmetric ones further from the vessel, depending on the array distance from the laser applicator. The proposed setup together with the investigation of an asymmetric configuration of sensors and vessels allowed to observe and quantify the vessel influence on the thermal gradient in the target and the cooling of the tissue caused by blood perfusion, simulated by heated water flow, in the region of the vessel. This result could be useful for clinical applications because tissue cooling by perfusion can limit the reproducible size of the ablation lesion.

REFERENCES

- [1] S. N. Goldberg, G. S. Gazelle, and P. R. Mueller, "Thermal ablation therapy for focal malignancy," *Amer. J. Roentgenol.*, vol. 174, no. 2, pp. 323–331, Feb. 2000.
- [2] M. G. Skinner *et al.*, "A theoretical comparison of energy sources - microwave, ultrasound and laser - for interstitial thermal therapy," *Phys. Med. Biol.*, vol. 43, no. 12, pp. 3535–3547, Dec. 1998.
- [3] N. Weiss *et al.*, "Temperature–density hysteresis in X-ray CT during HIFU thermal ablation: Heating and cooling phantom study," *Int. J. Hyperthermia*, vol. 30, no. 1, pp. 27–35, Feb. 2014.
- [4] K. F. Chu and D. E. Dupuy, "Thermal ablation of tumours: Biological mechanisms and advances in therapy," *Nat. Rev. Cancer*, vol. 14, no. 3, pp. 199–208, Mar. 2014.
- [5] M. Ahmed *et al.*, "Principles of and advances in percutaneous ablation," *Radiology*, vol. 258, no. 2, pp. 351–369, Feb. 2011.
- [6] S. A. Sapareto and W. C. Dewey, "Thermal dose determination in cancer therapy," *Int. J. Radiat. Oncol. Biol. Phys.*, vol. 10, no. 6, pp. 787–800, 1984.
- [7] I. A. Chang and U. D. Nguyen, "Thermal modeling of lesion growth with radiofrequency ablation devices," *Biomed. Eng. Online*, vol. 3, no. 1, 2004, Art. no. 27.
- [8] M. W. Dewhirst *et al.*, "Basic principles of thermal dosimetry and thermal thresholds for tissue damage from hyperthermia," *Int. J. Hyperthermia*, vol. 19, no. 3, pp. 267–294, Jan. 2003.
- [9] R. J. Stafford *et al.*, "Laser-induced thermal therapy for tumor ablation," *Crit. Rev. Biomed. Eng.*, vol. 38, no. 1, pp. 79–100, 2010.
- [10] R. K. Jain, "Temperature distributions in normal and neoplastic tissues during normothermia and hyperthermia," *Annals New York Acad. Sci.*, vol. 335, no. 1, pp. 48–66, Mar. 1980.
- [11] J. Crezee and J. J. W. Lagendijk, "Experimental verification of bio-heat transfer theories: Measurement of temperature profiles around large artificial vessels in perfused tissue," *Phys. Med. Biol.*, vol. 35, no. 7, pp. 905–923, Jul. 1990.
- [12] H.-W. Huang and T.-L. Horng, "Bioheat transfer and thermal heating for tumor treatment," in *Heat Transfer and Fluid Flow in Biological Processes*, Amsterdam, The Netherlands: Elsevier, 2015, pp. 1–42.
- [13] B. E. Lyons *et al.*, "Heat loss and blood flow during hyperthermia in normal canine brain I: Empirical study and analysis," *Int. J. Hyperthermia*, vol. 5, no. 2, pp. 225–247, Jan. 1989.
- [14] *Optical-Thermal Response of Laser-Irradiated Tissue*, A. J. Welch and M. J. C. van Gemert, Eds., Dordrecht, The Netherlands: Springer Netherlands, 2011.
- [15] C. J. Diederich, "Thermal ablation and high-temperature thermal therapy: Overview of technology and clinical implementation," *Int. J. Hyperthermia*, vol. 21, no. 8, pp. 745–753, Dec. 2005.
- [16] J. F. Verhey *et al.*, "Implementation of a practical model for light and heat distribution using laser-induced thermotherapy near to a large vessel," *Phys. Med. Biol.*, vol. 48, no. 21, pp. 3595–3610, Nov. 2003.
- [17] L. Consiglieri, I. dos Santos, and D. Haemmerich, "Theoretical analysis of the heat convection coefficient in large vessels and the significance for thermal ablative therapies," *Phys. Med. Biol.*, vol. 48, no. 24, pp. 4125–4134, Dec. 2003.
- [18] V. Muralidharan, C. Malcontenti-Wilson, and C. Christophi, "Effect of blood flow occlusion on laser hyperthermia for liver metastases," *J. Surgical Res.*, vol. 103, no. 2, pp. 165–174, Apr. 2002.
- [19] S. N. Goldberg *et al.*, "Ablation of liver tumors using percutaneous RF therapy," *Amer. J. Roentgenol.*, vol. 170, no. 4, pp. 1023–1028, Apr. 1998.
- [20] J. J. W. Lagendijk, "Hyperthermia treatment planning," *Phys. Med. Biol.*, vol. 45, no. 5, pp. R61–R76, May 2000.
- [21] G. Palumbo *et al.*, "Temperature profile of ex-vivo organs during radio frequency thermal ablation by fiber Bragg gratings," *J. Biomed. Opt.*, vol. 21, no. 11, Nov. 2016, Art. no. 117003.
- [22] V. Mishra *et al.*, "Fiber grating sensors in medicine: Current and emerging applications," *Sensors Actuators A Phys.*, vol. 167, no. 2, pp. 279–290, Jun. 2011.
- [23] G. Palumbo *et al.*, "Multidimensional thermal mapping during radiofrequency ablation treatments with minimally invasive fiber optic sensors," *Biomed. Opt. Express*, vol. 9, no. 12, Dec. 2018, Art. no. 5891.
- [24] S. Silvestri and E. Schena, "Optical-fiber measurement systems for medical applications," in *Optoelectronics - Devices and Applications*. Rijeka, Croatia: InTech, 2011.
- [25] D. J. Webb *et al.*, "First in-vivo trials of a fiber Bragg grating based temperature profiling system," *J. Biomed. Opt.*, vol. 5, no. 1, 2000, Art. no. 45.
- [26] G. Braschi *et al.*, "Monitoring of radiofrequency thermal ablation in liver tissue through fibre Bragg grating sensors array," *Electron. Lett.*, vol. 50, no. 14, pp. 981–983, Jul. 2014.
- [27] D. Tosi *et al.*, "Intra-tissue pressure measurement in ex vivo liver undergoing laser ablation with fiber-optic Fabry-Perot probe," *Sensors*, vol. 16, no. 4, Apr. 2016, Art. no. 544.
- [28] D. Polito *et al.*, "A needlelike probe for temperature monitoring during laser ablation based on fiber Bragg grating: Manufacturing and characterization," *J. Med. Device.*, vol. 9, no. 4, pp. 041006-1–041006-8, Dec. 2015.
- [29] F. M. Di Matteo *et al.*, "Feasibility of EUS-guided Nd:YAG laser ablation of unresectable pancreatic adenocarcinoma," *Gastrointestinal Endoscopy*, vol. 88, no. 1, pp. 168–174, Jul. 2018.
- [30] Q. Yu *et al.*, "Study on optical fiber Bragg grating temperature sensors for human body temperature monitoring," in *Proc. Symp. Photon. Optoelectronics*, 2012, pp. 1–4.
- [31] A. D. Kersey *et al.*, "Fiber grating sensors," *J. Lightw. Technol.*, vol. 15, no. 8, pp. 1442–1463, Aug. 1997.
- [32] K. O. Hill and G. Meltz, "Fiber Bragg grating technology fundamentals and overview," *J. Lightw. Technol.*, vol. 15, no. 8, pp. 1263–1276, Aug. 1997.
- [33] A. Usman *et al.*, "Determination of normal portal vein diameter on ultrasound scan among adults in northeastern Nigeria," *Int. Surgery*, vol. 5, no. 3, 2015, Art. no. 143.
- [34] R. Qasrawi *et al.*, "Anatomically realistic simulations of liver ablation by irreversible electroporation: Impact of blood vessels on ablation volumes and undertreatment," *Technol. Cancer Res. Treatment*, vol. 16, no. 6, pp. 783–792, Dec. 2017.
- [35] C. Debbaut *et al.*, "Analyzing the human liver vascular architecture by combining vascular corrosion casting and micro-CT scanning: A feasibility study," *J. Anatomy*, vol. 224, no. 4, pp. 509–517, Apr. 2014.
- [36] J. Heisterkamp, R. van Hillegersberg, and J. N. M. IJzermans, "Interstitial laser coagulation for hepatic tumours," *British J. Surgery*, vol. 86, no. 3, pp. 293–304, Mar. 1999.
- [37] J. J. W. Lagendijk, "The influence of bloodflow in large vessels on the temperature distribution in hyperthermia," *Phys. Med. Biol.*, vol. 27, no. 1, pp. 17–23, Jan. 1982.
- [38] S. N. Goldberg *et al.*, "Radio-frequency tissue ablation: effect of pharmacologic modulation of blood flow on coagulation diameter," *Radiology*, vol. 209, no. 3, pp. 761–767, Dec. 1998.
- [39] L. Chen *et al.*, "Effect of blood perfusion on the ablation of liver parenchyma with high-intensity focused ultrasound," *Phys. Med. Biol.*, vol. 38, no. 11, pp. 1661–1673, Nov. 1993.
- [40] J. Heisterkamp *et al.*, "Importance of eliminating portal flow to produce large intrahepatic lesions with interstitial laser coagulation," *British J. Surgery*, vol. 84, no. 9, pp. 1245–1248, Sep. 1997.
- [41] K. Pillai *et al.*, "Heat sink effect on tumor ablation characteristics as observed in monopolar radiofrequency, bipolar radiofrequency, and microwave, using ex vivo calf liver model," *Medicine (Baltimore)*, vol. 94, no. 9, pp. 1–10, 2015.
- [42] F. G. M. Poch *et al.*, "The vascular cooling effect in hepatic multipolar radiofrequency ablation leads to incomplete ablation ex vivo," *Int. J. Hyperthermia*, vol. 32, no. 7, pp. 749–756, Oct. 2016.
- [43] M. Seitz *et al.*, "Ex vivo and in vivo investigations of the novel 1,470 nm diode laser for potential treatment of benign prostatic enlargement," *Lasers Med. Sci.*, vol. 24, no. 3, May 2009, Art. no. 419.
- [44] Y. J. Rao, "Optical in-fiber Bragg grating sensor systems for medical applications," *J. Biomed. Opt.*, vol. 3, no. 1, Jan. 1998, Art. no. 38.
- [45] C. Cavaiola *et al.*, "Error of a temperature probe for cancer ablation monitoring caused by respiratory movements: Ex vivo and in vivo analysis," *IEEE Sens. J.*, vol. 16, no. 15, pp. 5934–5941, Aug. 2016.
- [46] P. Saccomandi *et al.*, "Linearly chirped fiber Bragg grating response to thermal gradient: from bench tests to the real-time assessment during in vivo laser ablations of biological tissue," *J. Biomed. Opt.*, vol. 22, no. 9, pp. 097002-1–097002-9, Sep. 2017.
- [47] E. De Vita *et al.*, "Temperature monitoring during radio frequency thermal ablation treatment on ex vivo perfused organ by fiber Bragg grating sensors," in *Proc. IEEE Int. Symp. Med. Meas. Appl.*, 2018, pp. 1–6.
- [48] A. Andreano *et al.*, "Microwaves create larger ablations than radiofrequency when controlled for power in ex vivo tissue," *Med. Phys.*, vol. 37, no. 6, pp. 2967–2973, May 2010.